

Two-Dimensional Simulations of Stimulated Brillouin Scattering in Laser Produced Plasmas

M. R. Amin and C. E. Capjack

Department of Electrical Engineering, University of Alberta, Edmonton, Alberta, Canada T6G 2G7

P. Frycz, W. Rozmus, and V. T. Tikhonchuk*

Department of Physics, University of Alberta, Edmonton, Alberta, Canada T6G 2J1

(Received 13 November 1992)

A system of electromagnetic and ion acoustic wave equations coupled via the ponderomotive force are solved numerically in a two-dimensional planar geometry. The competition between forward, side, and backward Brillouin scattering of the finite size laser beam is studied for the first time without the standard paraxial optics approximation. Simulations reveal a strong dependence of the scattered light characteristics on the geometry of the interaction region, the shape of the pump beam, and the ion acoustic wave damping. The main effects include side and forward scattering enhancement and a stimulation of collimated backward scattered radiation.

PACS numbers: 52.40.Nk, 52.35.Mw

Stimulated Brillouin scattering (SBS) is a parametric instability corresponding to the decay of an incident electromagnetic pump wave into an ion sound wave (ISW) and a second electromagnetic wave with a lower frequency propagating in a different direction [1]. Although SBS has been the subject of extensive experimental and theoretical studies for more than two decades [2], many features of the experimental results in laser plasmas are still not understood. These include observed low levels of SBS saturation, a complex temporal behavior, and a large fraction of side and forward scattered light. Part of the difficulty in understanding experimental results can be attributed to the use of one-dimensional (1D) SBS models in which geometric effects resulting from the finite size of the laser beam and the filamentation instability are not included. In this Letter, results are presented from a fully two-dimensional (2D) model which describes the interaction of a laser beam with a low frequency ISW. A unique feature of the model is that it does not rely on the use of a paraxial approximation [3] for the electromagnetic waves, thereby allowing a detailed resolution of the angular distribution of scattered radiation in the presence of filamentation and self-focusing instabilities [4].

We consider a 2D homogeneous rectangular plasma slab in the x - y plane. The pump electromagnetic wave propagates along the x direction and its electric field is polarized in the z direction. Scattered electromagnetic waves are allowed to propagate in every direction in the x - y plane, and are assumed to have the same polarization as the pump wave. The damping of all electromagnetic waves is assumed negligible. At the entrance line ($x = 0$) the pump wave has a hatlike distribution $E_0(y) = \frac{1}{2}E_0(\tanh\frac{y+a}{\delta} - \tanh\frac{y-a}{\delta})$, where a stands for the half-width of the beam, and δ characterizes the smoothness of the beam edges. The interaction length L in the x direction has been taken to be much smaller than the beam Rayleigh length k_0a^2 , where $k_0 = \omega_0/c$, ω_0 is the pump wave frequency, and c is the speed of

light. The propagation of the electromagnetic waves in the plasma has been described by the 2D wave equation for the time enveloped electric field $E(x, y, t)$ [5, 6] with outgoing boundary conditions,

$$\left[2i\frac{\omega_0}{c^2}\frac{\partial}{\partial t} + \nabla^2 + k_0^2\left(1 - \frac{n_e}{n_c}\right) \right] E = k_0^2\frac{\delta n_e}{n_c} E, \quad (1)$$

where n_c stands for the electron critical density and n_e is the background electron plasma density. The coupling between different electromagnetic waves has been introduced via the density perturbations δn_e , whose evolution has been described by the 2D acoustic wave equation with the ponderomotive force produced by the pump and scattered electromagnetic waves,

$$\left[\frac{\partial^2}{\partial t^2} - 2\eta\nabla^2\frac{\partial}{\partial t} - c_s^2\nabla^2 \right] \frac{\delta n_e}{n_e} = \frac{c_s^2}{16\pi n_c T_e} \nabla^2 |E|^2 + S(x, y, t), \quad (2)$$

where T_e is the electron plasma temperature and c_s is the ion acoustic speed. The ion acoustic wave damping is represented by the phenomenological viscous term [5, 6] with a coefficient η . This approximation for the damping correctly describes the competition between forward and backward SBS. The ion sound waves participating in forward SBS are unaffected by the damping due to the small values of \mathbf{k} , and the damping for the resonantly driven ISW by the backward SBS can be properly adjusted via the magnitude of the damping coefficient η . Small amplitude random density perturbations are used as initial conditions. During the simulation, the level of fluctuations has been kept approximately constant by periodically adding the necessary amount of noise, which is represented by the random δ -correlated source term S in Eq. (2). Details of the numerical solution of Eqs. (1) and (2) were presented in Ref. [6]. We introduce the dimensionless pump wave intensity $I_0 = E_0^2/8\pi n_c T_e$ and the dimensionless background electron plasma den-

sity $N_0 = n_e/n_c$. All spatial scales are measured in units of the pump vacuum wavelength $\lambda_0 = 2\pi c/\omega_0$, while the time intervals are measured in units of $(k_0 c_s)^{-1}$. Two parameter sets have been used in the simulations to be described. In one case, the pump beam is chosen to be relatively wide ($a = 50\lambda_0$) with a smooth lateral intensity distribution. This case could be expected to model the 1D situation. The other case ($a = 10\lambda_0$) corresponds to the interaction of a laser beam filament ("hot spot") with a preformed homogeneous plasma.

The damping of ISW is characterized by the dimensionless parameter $\Gamma = 2\eta k_0(1 - N_0)^{1/2}/c_s$, which corresponds to the damping to frequency ratio of the ISW participating in the backward SBS. The ratio of the total power that is emitted into the rear semicircle ($\frac{1}{2}\pi < \theta < \frac{3}{2}\pi$) divided by the input power is shown in Fig. 1. The characteristic temporal evolution of the backscattered radiation is shown in Fig. 1(a) for the case of relatively

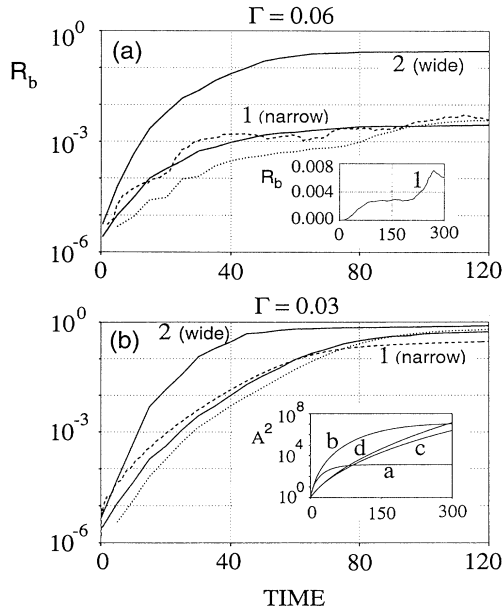


FIG. 1. The temporal dependence of the reflectivity in the rear semicircle $R_b(k_0 c_s t) = P_0^{-1} \int_{\pi/2}^{3\pi/2} d\theta Q(\theta, t)$ for the case of (a) strong ($\Gamma = 0.06$) and (b) weak ($\Gamma = 0.03$) ion acoustic wave damping. The other parameters of the simulations are the following: $I_0 = 0.045$, $N_0 = 0.2$, $L = 35.5\lambda_0$, $\delta = 2.2\lambda_0$; $a = 10\lambda_0$ for curves 1 and $a = 50\lambda_0$ for curves 2. The dashed curves correspond to the 1D KdV runs while the dotted curves are for the 1D version of the 2D code with the same parameters. The inset panel in (a) shows the late time behavior of the reflectivity R_b for the case of strong ion acoustic damping, curve 1. The inset panel in (b) shows the square of the linear amplification coefficient A , expression (4) in the text, as a function of time. Curves *a* and *b* are drawn for exactly backscattering ($\theta = 180^\circ$) while curves *c* and *d* are for near forward scattering ($\theta = 30^\circ$). The parameters of curves *a* and *c* are the same as the parameters of curve 1 in (a) while curves *b* and *d* correspond to curve 1 in (b).

strongly damped ion acoustic waves $\Gamma = 0.06$, and in Fig. 1(b) for the case of weak damping $\Gamma = 0.03$. Corresponding results obtained by running the present code in a 1D mode are given by the dotted curves in Fig. 1. An unexpected feature of these results is the close agreement with the 2D narrow pump case (curves 1). It will be shown that the much larger reflectivity, as compared to 1D results, for the wide beam runs ($a > L$, curves 2) can be attributed to a substantial amount of side scattering. Also included in Fig. 1 are results obtained with a 1D model of SBS based on the driven Korteweg-de Vries (KdV) equation [7] for ISW (dashed curves). These are in close agreement with the 2D results for the narrow pump case, similar to 1D results with linear ISW. The saturation of 1D reflectivity which is predicted for the case of a weakly damped ISW in Fig. 1(b) is caused by the nonlinear effects included in the KdV equation [7]. It is also interesting to note that the 2D simulations display a much more complicated long time behavior [cf. inset panel in Fig. 1(a)]. The backscattered signal is seen to grow after a long period of an apparent saturation. This final signal exceeds the convective saturation level by 2 to 3 times and has a very narrow angular distribution which is approximately equal to the pump beam width. This unexpected behavior resembles pump wave reflection by

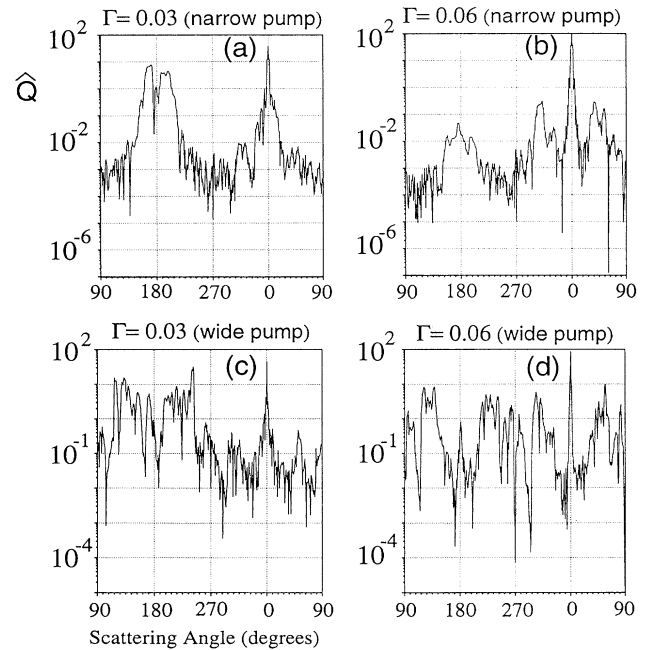


FIG. 2. The angular distribution of the electromagnetic wave power emitted from the plasma slab in the far field zone $\hat{Q} = Q(\theta, t)/(cn_c T_e/k_0)$. Panels (a) and (c) correspond to the parameters of curve 1 (narrow pump) and curve 2 (wide pump), respectively, in Fig. 1(b) while panels (b) and (d) correspond to the parameters of curve 1 (narrow pump) and curve 2 (wide pump), respectively, in Fig. 1(a). Panels (a), (c), and (d) are for time $k_0 c_s t = 120$ while panel (b) is for time $k_0 c_s t = 180$.

phase conjugation [8].

Figure 2 shows the angular distribution of the scattered electromagnetic field $Q(\theta, t)$ in the far field (Fraunhofer) zone. The quantity $Q(\theta, t)$ is the electromagnetic field power emitted in the unit angle from the interaction region in the direction defined by the scattering angle θ at time t . The nonscattered light is emitted in a narrow cone $\Delta\theta \approx \lambda_0/a \lesssim 10^\circ$. The scattered signal originates from the interaction of the incident electromagnetic wave with the ISW. The ISW grows from noise which is maintained at a level $\langle \delta n_e^2 \rangle^{1/2}/n_e \lesssim 10^{-3}$ throughout a run. The scattered electromagnetic power from the initial noise level of the ISW is given by the formula

$$Q_0 = P_0 (k_0^3/8\pi) L (1 - N_0)^{-1/2} \langle |\delta n_{\mathbf{k}}|^2 \rangle / n_e^2, \quad (3)$$

$$A(\theta, t) = -\frac{1}{G} + \frac{1}{2\pi i G} \int_{-i\infty+\sigma}^{+i\infty+\sigma} \frac{dp}{p} (1+p) \exp \left[2k_0 c_s t \Gamma p \sqrt{1 - N_0} \sin^2 \frac{\theta}{2} + \frac{G}{1+p} \right], \quad (4)$$

$\sigma > 0$, and $G(\theta) = I_0 N_0 k_0 \ell(\theta) / 8\Gamma \sin(\theta/2) \sqrt{1 - N_0}$ is the stationary SBS gain and $\ell(\theta)$ is the interaction length along the direction of propagation of the scattered light. The temporal dependence of the square of the SBS amplification coefficient is illustrated in the inset panel in Fig. 1(b).

Expression (4) predicts that backscattered SBS will have the fastest growth rate. In the case of Figs. 2(a) and 2(c), the stationary amplification coefficient $A_{st} = (1/G)(\exp G - 1)$ is sufficiently large for $\theta = \pi$ that the backscatter will saturate at a relatively high level. Because of pump depletion, scattering in other directions will be suppressed. The characteristic angular width of the backscattered light ($\Delta\theta \approx 2a/L$) is determined by the angular range over which the gain length of the backward traveling SBS is maximized.

If the ion acoustic wave damping is large and the amplification coefficient $A_{st}(\theta = \pi) \lesssim 10^2$, then the backscatter saturates convectively at a low level [cf. Fig. 2(b)] without pump depletion occurring. Both side and forward scattering have an opportunity to grow and the temporal behavior of SBS depends on the relation between the pump width a and the length of the interaction region L . Side scatter is dominant for the case of a wide pump and a short interaction region ($a > L$) [cf. Fig. 2(d)]. In that case the maximum of the amplification coefficient (4) is slightly shifted from $\theta = \frac{1}{2}\pi$ toward larger angles. This large contribution from side scattering is the reason why the integrated backscattered power [curve 2 in Fig. 1(a)] is considerably larger than the predictions from a 1D analysis. In the limit of a long interaction region ($L > a$), the effect of ponderomotively produced density disturbances becomes more important and forward SBS plays a dominant role. Figure 2(b) shows the bulk of the scattered radiation to be emitted within an angular interval $\theta \approx \frac{1}{3}\pi$, with a peak occurring at $\theta \approx \frac{1}{4}\pi$. The physical explanation for this observed peak is that the ponderomotive force that results from the steep edges of the pump beam drives transverse density perturbations

where $P_0 = (c/8\pi) \int dy |E_0|^2$ is the pump beam power and $\langle |\delta n_{\mathbf{k}}|^2 \rangle$ is the correlation function of the density fluctuation Fourier spectrum. The magnitude of Q_0 is about $10^{-5}P_0$ in the simulations that are performed. The forward Brillouin scattering grows both from the imposed stationary random density fluctuations and from fluctuations produced by the pump beam spatial inhomogeneity. The ponderomotive force is maximized at the beam edges and builds up the ion density disturbances (cf. Fig. 3), which in turn seed forward SBS.

The linear theory of the convective nonstationary SBS predicts the following time dependence of the scattered signal: $Q(\theta, t) = Q_0 |A(\theta, t)|^2$, where A is the amplification coefficient for the resonant SBS interaction

with scale lengths of the order of λ_0 to $2\lambda_0$. The phase matching conditions for forward scattering are therefore satisfied for $\theta \leq \frac{1}{3}\pi$. Because the growth rate is an increasing function of θ , the maximum intensities appear on the cone edges as is seen in Fig. 2(b). The forward SBS saturates after a time $t_{sat} \approx L/c_s$, when the ISW passes the interaction region.

Figures 3 and 4 display snapshots of the spatial distribution of the ion density fluctuations inside the plasma slab. Figure 3 gives the ion density distribution for the case of strong ion acoustic damping and a narrow pump beam just after the convective saturation of the backscattered signal. The strong ponderomotive force occurring at the steep edges of the pump beam produces a transient plasma response which results in density fluctua-

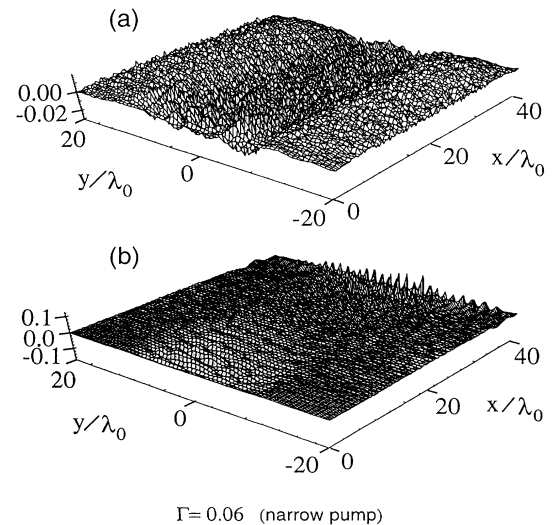


FIG. 3. The spatial distribution of the ion density fluctuations $\delta n_e(x, y, t)/n_e$ in the plasma slab for the parameters of curve 1 in Fig. 1 (a) at time $k_0 c_s t = 60$ for panel (a) and 270 for panel (b). (The case of strong ion acoustic damping.)

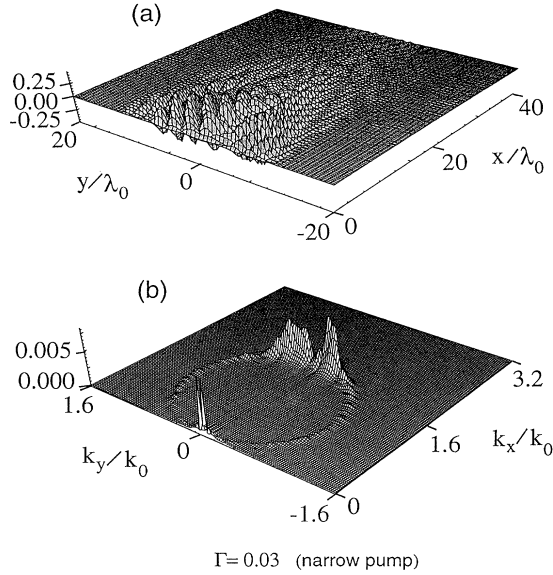


FIG. 4. The spatial distribution of the ion density fluctuations in the plasma slab $\delta n_e(x, y, t)/n_e$ [panel (a)] and their Fourier spectrum $|\delta n_e(k_x, k_y)|/n_e$ [panel (b)], for the parameters of curve 1 in Fig. 1(b) at time $k_0 c_s t = 120$ (weak ion acoustic damping case).

tions that favor forward SBS growth. As the ion density waves propagate across and out of the simulation box, the interaction region for forward scattering shrinks. This gives more room for amplification of the backscattered signal [cf. Fig. 3(b)]. The additional increase of the level of backward SBS is produced by density fluctuations near the forward boundary. The level of small scale density fluctuations, however, remains much smaller than the amplitudes of the large scale disturbances responsible for the forward SBS. The case where the damping of ISW is weak [Fig. 4(a)] demonstrates the opposite situation. The amplitude of small scale fluctuations participating in backward SBS is now much larger than the plasma channel depth. This fact becomes even more evident in Fig. 4(b), where the Fourier spectrum of the density fluctuations is shown. The large amplitude components have $k_x \approx 2k_0$ and correspond to the backward scattering, whereas the two narrow lines nearby the origin are related to the density channel formation and lead to the modulations of the angular distribution of the backscattered light.

In conclusion, the 2D simulations reveal several different scenarios of the temporal evolution of SBS, which depend on the value of the stationary backscatter amplification coefficient $A_{st}(\theta = \pi)$ and the ratio of the

beam size to the interaction length a/L . In the case of large values of $A_{st}(\theta = \pi) \gtrsim 10^2 - 10^3$, strong backscatter and pump beam depletion take place and the angle integrated reflectivity is in a good agreement with 1D theory. However, the angular distribution of the scattered light is much wider than that of the pump beam. For the smaller values of $A_{st}(\pi)$ and a short interaction region ($a > L$), sideward SBS dominates and backscattering saturates at a very low level. Finally, in the case of a relatively small backscatter amplification coefficient and a long interaction region, strong forward SBS takes place. The last case is in a qualitative agreement with the recent observations of forward SBS in the experiments with long scale preformed plasmas [9]. This study has addressed the case where the self-focusing length of the beam is much longer than the length of the interaction region. The case where SBS coexists with incident beam self-focusing will be described in a future publication.

This work was partially supported by the Natural Sciences and Engineering Research Council of Canada.

* On leave from P. N. Lebedev Physics Institute, Russian Academy of Sciences, Moscow, Russia.

- [1] W. L. Kruer, *The Physics of Laser Plasma Interactions* (Addison-Wesley, New York, 1988).
- [2] H. A. Baldis, E. M. Campbell, and W. L. Kruer, in *Handbook of Plasma Physics*, edited by A. Rubenchik and S. Witkowski (North-Holland, Amsterdam, 1991), Vol. 3, p. 361.
- [3] R. Rankin, R. Marchand, and C. E. Capjack, *Phys. Fluids* **31**, 2327 (1988); A. J. Schmitt, *Phys. Fluids* **31**, 3079 (1988); C. Aldrich, J. L. Norton, G. D. Pollak, and J. M. Wallace, *Phys. Fluids* **31**, 1249 (1988); B. I. Cohen, B. F. Lasinski, A. B. Langdon, and J. C. Cummings, *Phys. Fluids B* **3**, 766 (1991).
- [4] G. A. Askar'yan, *Zh. Eksp. Teor. Fiz.* **42**, 1567 (1962) [*Sov. Phys. JETP* **15**, 1088 (1962)]; P. Kaw, G. Schmidt, and T. Wilcox, *Phys. Fluids* **16**, 1522 (1973); W. L. Kruer, *Comments Plasma Phys. Controlled Fusion* **9**, 63 (1985).
- [5] A. A. Andreev, N. E. Andreev, A. N. Sutyagin, and V. T. Tikhonchuk, *Fiz. Plazmy* **15**, 944 (1989) [*Sov. J. Plasma Phys.* **15**, 546 (1989)].
- [6] P. Frycz, W. Rozmus, J. Samson, V. T. Tikhonchuk, and R. Rankin, *Comments Plasma Phys. Controlled Fusion* **15**, 19 (1992).
- [7] W. Rozmus, M. Casanova, D. Pesme, A. Heron, and J. -C. Adam, *Phys. Fluids B* **4**, 576 (1992).
- [8] R. H. Lehberg, *Phys. Rev. Lett.* **41**, 863 (1978).
- [9] S. H. Batha, K. S. Bradley, H. A. Baldis, R. P. Drake, K. Estabrook, T. W. Johnston, and D. Montgomery, *Phys. Rev. Lett.* **70**, 802 (1993).